

Different trends in Antarctic temperature and atmospheric CO₂ during the last glacial

Peisong Zheng^{1,2}, Joel B. Pedro^{3,4}, Markus Jochum⁵, Sune O. Rasmussen⁶, Zhongping Lai^{1,7*}

¹ Guangdong Provincial Key Laboratory of Marine Biotechnology, Institute of Marine Sciences, Shantou University, Shantou 515063, China.

² School of Earth Sciences, China University of Geosciences, Wuhan 430074, China.

³ Australian Antarctic Division, Kingston, Tasmania, Australia.

⁴ Australian Antarctic Program Partnership, University of Tasmania, Hobart, Tasmania, Australia.

⁵ TeamOcean, Niels Bohr Institute, University of Copenhagen, Copenhagen, Denmark.

⁶ Centre for Ice and Climate, Section for the Physics of Ice, Climate, and Earth, Niels Bohr Institute, University of Copenhagen, Copenhagen, Denmark.

⁷ Three Gorges Research Center for Geohazards of MOE, China University of Geosciences, Wuhan 430074, China.

Corresponding author: **Zhongping Lai** (zhongping.lai@yahoo.com)

Key Points:

- The Antarctic warming rate during Antarctic Isotope Maxima significantly decreased as the climate cooled toward the glacial maximum.
- The Antarctic warming rate during Antarctic Isotope Maxima is insensitive to whether the warming coincides with a Heinrich event.
- In contrast, the millennial-scale CO₂ rise is insensitive to long-term glacial cooling but sensitive to the presence of Heinrich events.

22 **Abstract**

23 Using Antarctic ice-core records, we determine for each Antarctic Isotope Maximum (AIM) of
24 Marine Isotope Stage 3 (MIS-3: ca. 28,000 to 59,000 years before present) the rates and
25 durations of warming and atmospheric CO₂ rise. We find that the AIM warming rates
26 significantly decrease as the climate cools from early to late MIS-3. In contrast, the rate of
27 CO₂ rise during AIMs shows no significant trend across this interval. We further find that the
28 AIM warming rate is not sensitive to Heinrich (H) events, contrasting with CO₂, which rises for
29 significantly longer time (compared to the temperature rise) during AIMs which coincide with H
30 events. These distinct Antarctic temperature and CO₂ responses to varying background climate
31 and H events challenge the view that millennial-scale CO₂ and Antarctic temperature changes are
32 dominated by the same physical processes, suggesting an important contribution of low-to-mid-
33 latitude processes to the CO₂ rises.

34
35 **Plain Language Summary**

36 Glacial climate is characterized by millennial-scale variations in polar temperature and
37 atmospheric CO₂ concentration. Over the last two decades, a consistent explanation of the
38 temperature changes has emerged, but no such consensus exists with regard to CO₂. However,
39 due to the similarity of their records it is frequently proposed that CO₂ and Antarctic temperature
40 were controlled by the same processes. Here we present a new analysis of millennial-scale
41 Antarctic warming and CO₂ rise based on ice-core data. Our results show that during the latter
42 half of the glacial period, the Antarctica warming rate decreased as the climate cooled, but it was
43 not affected by occasional massive iceberg discharges (known as Heinrich events) that had a
44 dramatic impact on northern hemisphere climate. On the other hand, the rate of CO₂ change was

45 insensitive to the glacial cooling trend, but the CO₂ rise was sensitive to the occurrence of
46 Heinrich events. This suggests that on top of the processes that control millennial-scale Antarctic
47 temperature variations and also play a role for CO₂ levels, there are other processes (possibly of
48 extra-polar or terrestrial origin) that are important for the CO₂ dynamics.

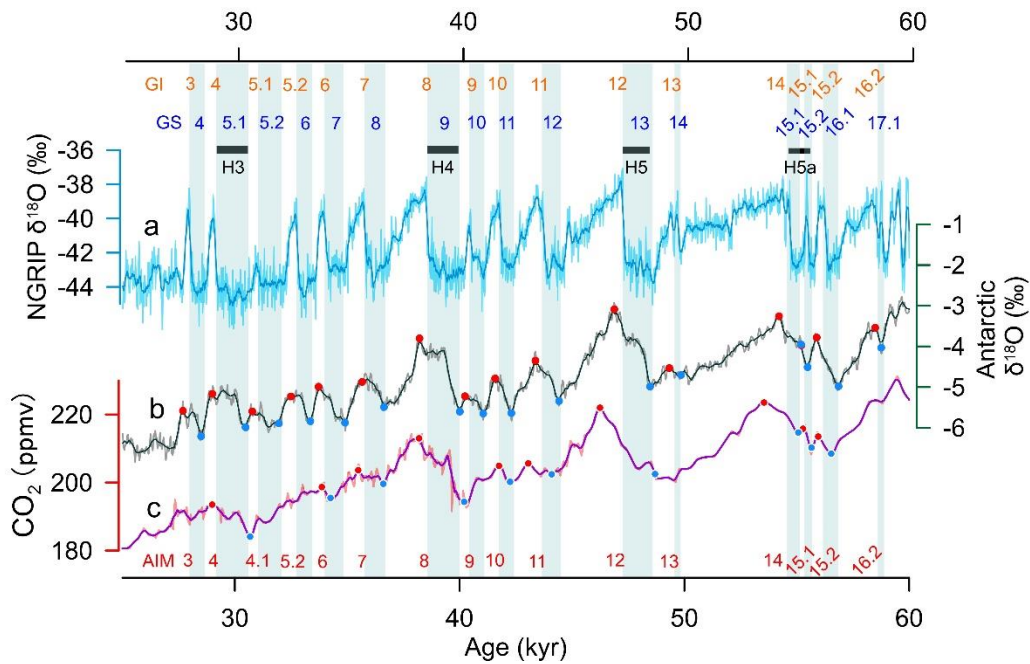
49 **1 Introduction**

50 Antarctic Isotope Maximums have a systematic relationship with the Dansgaard-
51 Oeschger (DO) oscillations recorded in Greenland ice cores during the last glacial period
52 (EPICA, 2006). The cold (Greenland stadial: GS) phase of the DO oscillation in Greenland
53 coincides with AIM warming in Antarctica and the warm (Greenland interstadial: GI) phase of
54 the DO coincides with AIM cooling (Figure 1). According to the bipolar ocean seesaw
55 hypothesis (Stocker & Johnsen, 2003), this interhemispheric coupling results from changes in
56 northward heat transport by the Atlantic Meridional Overturning Circulation (AMOC): GSs are
57 associated with a weak AMOC, reduced northward heat transport in the Atlantic and warming in
58 the South Atlantic. AIM warming in Antarctica follows, after a centennial-scale lag, as the South
59 Atlantic warm anomaly spreads through the upper to intermediate-depth ocean and is gradually
60 mixed across the Antarctic Circumpolar Current, in turn melting back Southern Ocean sea ice
61 and increasing atmospheric heat transport to Antarctica (see Pedro et al., 2018; for a view that
62 places more emphasis on buoyancy forcing see Thompson et al., 2019).

63 Previous work, based on the EPICA Dronning Maud Land (EDML) ice core, identified a
64 strong linear relationship ($r^2 = 0.85$) between the duration of GSs and the amplitude of
65 corresponding AIMs during MIS-3 (EPICA, 2006). The linear relationship suggested that the
66 amplitude of AIM warming depends only on the duration of Greenland stadials and that the
67 operation of the bipolar seesaw is not significantly influenced either by the evolution of the

68 climate state during the glacial, nor by the presence of H events. However, only eleven of the
69 sixteen MIS-3 AIMs were considered in that analysis and more recent studies propose that the
70 bipolar seesaw is sensitive to background climate (Capron et al., 2010; Margari et al., 2010), and
71 the presence of H events (Margari et al., 2010). However, these sensitivities have not previously
72 been quantified or statistically assessed.

73 The apparent similarity between atmospheric CO₂ concentrations (hereafter CO₂) and
74 Antarctic temperature change in the Antarctic ice-core record (Figure 1) has been hypothesized
75 to result from a common cause, such as changes in wind-driven upwelling (Anderson et al.,
76 2009; Anderson & Carr, 2010; Menviel et al., 2018; Toggweiler et al., 2006), or changes in the
77 formation of Antarctica Bottom Water (AABW, Menviel et al., 2015). In both cases, the release
78 of CO₂ and heat involve coupled Southern Ocean processes: increased ventilation of relatively
79 warm and carbon-rich sub-surface waters in the Southern Ocean (Bauska et al., 2018; Gottschalk
80 et al., 2019; Jaccard et al., 2016; Skinner et al., 2020); and/or increased poleward heat transport
81 accompanying the AABW formation and CO₂ ventilation (Menviel et al., 2015). However, there
82 are two obvious differences between the millennial-scale CO₂ and Antarctic temperature
83 changes: a) CO₂ maximums associated with Heinrich stadials (HS, defined here as GS containing
84 a H event) visibly lag the peak of the corresponding AIM events (Figure 1; Bereiter et al., 2012);
85 and, b) CO₂ rises during non-Heinrich stadials (nHS), if resolved at all, are thought to be of
86 lower amplitude than those during HS (Ahn & Brook, 2014). However, as with the sensitivity of
87 AIM warming to background climate and H events, a robust statistical assessment of these CO₂
88 features is lacking. Thus, we constrain for each MIS-3 AIM the amplitude and duration of the
89 AIM warming phase and CO₂ rise. We then test the sensitivities of AIM warming and CO₂ rise
90 to the changes in background climate state and the presence of H events.



91

92

Figure 1. Millennial-scale climate events and atmospheric CO₂ variations for the MIS-3. a.

93

The oxygen isotope ratio ($\delta^{18}\text{O}$) from the North Greenland Ice Core Project (NGRIP) ice core, as

94

a proxy for Greenland temperature (NGRIP, 2004; Svensson et al., 2008). **b.** The Antarctic five-

95

core averaged $\delta^{18}\text{O}$ record (Buizert et al., 2018). **c.** The composite Antarctic ice core CO₂ record

96

(Bereiter et al., 2012). The red and blue dots in **b** and **c** show the identified AIM and CO₂

97

maxima and minima (see text for definitions). **b** is on the WD2014 timescale, all other

98

records were transferred to the WD2014 time scale by stretching the GICC05/AICC2012 age to

99

1.0063 times (Buizert et al., 2015). The Greenland stadials and interstadials events are numbered

100

following Rasmussen et al. (2014), the timing of Greenland climate transition is from Buizert et

101

al. (2015) and WAIS (2015). Timespan of the H events are marked by the horizontal gray bars.

102

The AIM event number is following EPICA (2006) and extended to AIM 16.2.

103

104 **2 Methods and results**

105 **2.1. AIM temperature rise**

106 We use the recently published Antarctic five-core averaged $\delta^{18}\text{O}$ stack (in WD2014
107 timescale; Buizert et al., 2014) to determine the individual MIS-3 AIM warming amplitudes. To
108 exclude uncertainties associated with $\delta^{18}\text{O}$ -temperature transformation (Jouzel et al., 2013;
109 Landais et al., 2015), we use per mille (‰) $\delta^{18}\text{O}$ change as our unit of measure for AIM warming
110 amplitude. EPICA (2006) concludes that AIM warming amplitude is only controlled by the
111 duration of the corresponding GS; i.e. that the AIM warming rate is constant. To test this result,
112 we go a step further than EPICA (2006) and define here the AIM amplitude divided by the GS
113 duration as the bipolar seesaw (BPS) warming. The GS durations are obtained from previous
114 work (Buizert et al., 2015).

115 To obtain a robust estimate for the bipolar seesaw warming rate and its uncertainty, a
116 Monte Carlo (MC) Methods is used: in every iteration, the maximums and minimums of each
117 AIM are determined from a randomly perturbed version of the five-core averaged $\delta^{18}\text{O}$ record
118 which is smoothed with a 200-yr moving average before calculating the BPS warming rate of
119 each AIM. The randomly perturbed $\delta^{18}\text{O}$ record is created by drawing values from the normal
120 distribution of the five-core averaged $\delta^{18}\text{O}$ record with standard deviation set at 0.12‰ (found as
121 the standard deviation of the residual of the smoothed data relative to the unsmoothed one).
122 Considering the 100 to 200 yr lag of the onsets and ends of AIM events relative to Greenland GS
123 and GI transitions (Svensson et al., 2020; WAIS, 2015), we conservatively search for the isotope
124 maximums and minimums in a 300 yr window starting at the time of the corresponding
125 Greenland climate transition (the window is not allowed to cross the adjacent Greenland climate

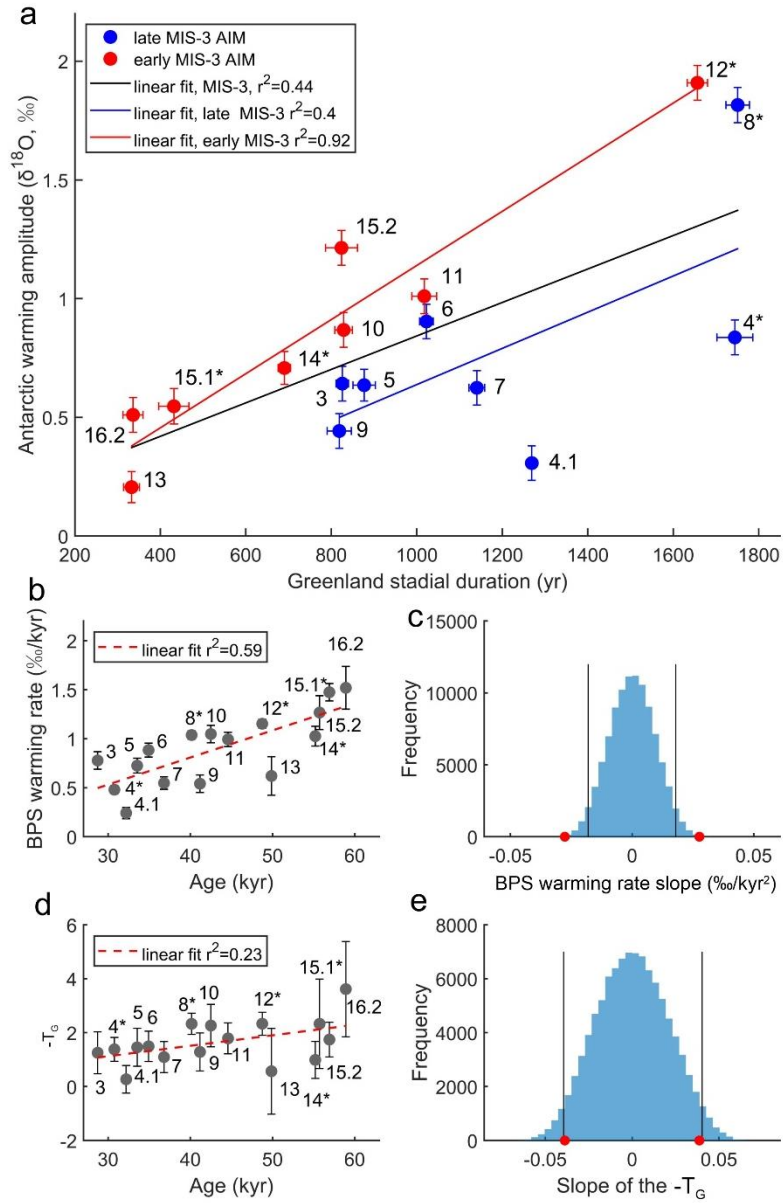
126 transition). After 100,000 iterations the median BPS warming rate for each AIM is used as the
127 output (Figure 2a), and the 95% confidence interval (CI) of the MC generated rates of each AIM
128 is used as the estimate of uncertainty range.

129 In contrast to the results of EPICA (2006), we do not observe a strong linear correlation
130 between GS duration and AIM amplitude (Figure 2a). Instead, our data suggest a lower BPS
131 warming rate during late MIS-3 than during early MIS-3 (Figure 2a, S1). To test if this reduction
132 is systematic, we plot the BPS warming rates against the AIM ages (defined as the onset of the
133 corresponding Greenland stadial). A clear decline in the warming rate across MIS-3 is observed
134 (Figure 2b). The significance of the observed slope is evaluated by comparing it with the slopes
135 generated from randomly permuting the BPS warming rate data points (keeping the AIM ages)
136 and re-calculating the resulting slopes 100,000 times. Only 0.06% of the absolute value of the
137 randomly generated slopes are larger than that obtained from the actual data (Figure 2c),
138 demonstrating the declining trend of BPS warming rate during MIS3 is significant.

139 Following EPICA (2006), our analysis above assumes that the BPS warming rate is
140 linear. If the AIM warming instead rises asymptotically, as predicted by the “minimum
141 thermodynamic seesaw model” (Margari et al., 2010; Stocker & Johnsen, 2003), then our
142 definition of the BPS warming rate could be biased low for longer GS. To test whether our result
143 holds under the assumption of an asymptotic rather than linear temperature increase during AIMS
144 we repeat our analysis fitting the warming phase of each AIM using the minimum
145 thermodynamic seesaw model (Stocker & Johnsen, 2003; Figure S2): $\Delta T_S = \Delta T_N (e^{-t/\tau} - 1)$, where
146 ΔT_S and ΔT_N are the amplitude of southern warming and northern cooling respectively, t is the
147 time since the start of the stadial, and τ is the equilibration timescale of the seesaw system,
148 estimated as 1120 yr (Margari et al., 2010; Stocker & Johnsen, 2003). We use isotope units

149 rather than temperature, and introduce the constant $-T_G$ to replace ΔT_N , representing the
150 amplitude of northern temperature (isotope) drop that gives the best fit to the observed AIM
151 isotope growth rate (note the $-T_G$ and ΔT_N have opposite sign). With τ kept constant, the shape of
152 the fitted curve is determined by $-T_G$, with smaller $-T_G$ corresponding to slower rises (Figure S3).
153 Similar to the linear case, Monte Carlo Methods is applied, and $-T_G$ of each AIM is determined
154 as the median of 100,000 iterations (Figure 2d).

155 Like the linear assessment of BPS warming rate, a slope showing the decline of $-T_G$
156 toward the glacial maximum is observed (Figure 2d). To test the significance of the slope, we
157 randomly permute the $-T_G$ values and re-calculate the slope 100,000 times and find that the
158 absolute value of the random slopes is larger than the value found from data in only 4.9% of the
159 cases, (Figure 2e), suggesting that $-T_G$ has a significant trend during MIS-3. This could be due to
160 a weakening of efficiency of the bipolar seesaw or a reduction of the driving ΔT_N , but as the
161 latter is not found in the reconstruction of northern temperature (Kindler et al., 2014), we
162 conclude that the bipolar seesaw was indeed weakening significantly during MIS-3 both under
163 the Stocker and Johnsen (2003) minimum thermodynamic seesaw model and that of linear AIM
164 warming rates (EPICA, 2006).



165

166 **Figure 2. The BPS warming rate results. a.** Greenland stadal duration and Antarctic warming
 167 amplitude, the AIM nomenclature is following EPICA (2006) and has been extended to AIM
 168 16.2. The error bar shows the uncertainty of GS duration (Buizert et al., 2015; WAIS, 2015) and
 169 the 95% CI of the amplitude. **b.** The BPS warming rate plotted against the age of the AIM. The
 170 error bar shows the range of 95% CI. **c.** The distribution of the slopes of the randomly permuted
 171 BPS warming rates, the red circle marks ± 1 time the slope observed from **b**, the 2.5% and 97.5%

172 fractile of the randomly generated slope are marked by vertical black lines. **d, e.** The same as **b, c**
173 for $-T_G$ instead of the BPS warming rate.

174

175 To test the sensitivity of AIM warming to H events we group the BPS warming rates and
176 $-T_G$ values for each AIM into HS and nHS categories (Figure S1). A Student's t-test shows no
177 significant difference (at 95% significance level) between HS and nHS BPS warming rates or $-$
178 T_G . These results suggest that the processes controlling Antarctic warming are insensitive to the
179 H events.

180 Our result of a weakening bipolar seesaw during MIS-3 is robust to replacing Greenland
181 stadial durations with the duration of the corresponding Antarctic isotope rise (the time between
182 the identified isotope minimum and maximum, Table S1). Removing the long-term signal
183 represented by 20,000 yr smoothing of the five-core averaged isotope data also does not change
184 the conclusions (Table S1, Figure S4). We also carried out the analysis of the BPS warming rate
185 and $-T_G$ on the individual ice-core records going into the five-core averaged data set: West
186 Antarctic Ice Sheet Divide (WDC; WAIS, 2013, 2015), European Project for Ice Coring in
187 Antarctica (EPICA) in the interior of Dronning Maud Land (EDML; EPICA, 2006), Talos Dome
188 (Landais et al., 2015; Stenni et al., 2011), EPICA Dome C (EDC; EPICA 2004), and Dome Fuji
189 (Fuji; Kawamura et al., 2007; Watanabe et al., 2003). Similar results are obtained (Table S1,
190 Figure S4). Although the EDML record may reflect more low-latitude and atmospheric signals
191 (Landais et al., 2015), our results show that in terms of the overall bipolar seesaw response, it is
192 not systematically different from other Antarctic ice cores. This is consistent with the conclusion
193 that a spatially homogeneous oceanic component of the AIM events related to the

194 thermodynamic seesaw response is the first and dominant principle component of the AIM
195 variability (Buizert et al., 2018).

196 **2.2. Millennial CO₂ rise:**

197 We determine the amplitude of MIS-3 millennial-scale CO₂ rise using the composite CO₂
198 record (on the AICC2012 timescale; Bereiter et al., 2015; Figure 1, S5). The MIS-3 section of
199 the composite CO₂ record consists of the Siple Dome (20 to 40 kyr BP; Ahn & Brook, 2014) and
200 Talos Dome (40 to 60 kyr BP; Bereiter et al., 2012) records. To avoid the influence of different
201 gas smoothing between ice cores, the CO₂ data is smoothed using a 300 yr moving average,
202 which is larger than the mean resolution of both CO₂ records (96 and 246 for Siple and Talos
203 Dome respectively). We note that there is a systematic offset between the two CO₂ records
204 (Bereiter et al., 2012) with a junction point (at about 40 kyr BP, Figure S5), this offset does not
205 fall within a period of assessed CO₂ rise, so it does not affect any of our derived CO₂ amplitudes.

206 Considering the CO₂ peak could lag the abrupt DO warming by several hundred to a
207 thousand years (Bereiter et al., 2012; Figure S5), we here extend the search window for the CO₂
208 maximums and minimums to 100 yr prior and 1000 yr after the Greenland climate transition. We
209 use the timing of Greenland climate transitions defined in Greenland $\delta^{18}\text{O}$ and Ca⁺ data
210 (Rasmussen et al., 2014).

211 In calculating the amplitudes and rates of MIS-3 CO₂ rise, we assess only those CO₂ rises
212 with amplitudes significantly larger than the measurement uncertainty (at the 95% level, Figure
213 S6). A total ten CO₂ rise are identified, five for the HS (DO 4, 8, 12, 14, 15.1) and five for the
214 nHS periods (DO, 6, 7, 10, 11, 15.2, Figure 1, 3a). We here focused on the overall CO₂ response

215 and defined the rate of CO₂ rise (Figure 3b) as CO₂ amplitude divided by the duration of the rise.
216 The CO₂ rate and its uncertainty are estimated by similar MC method of temperature rates.

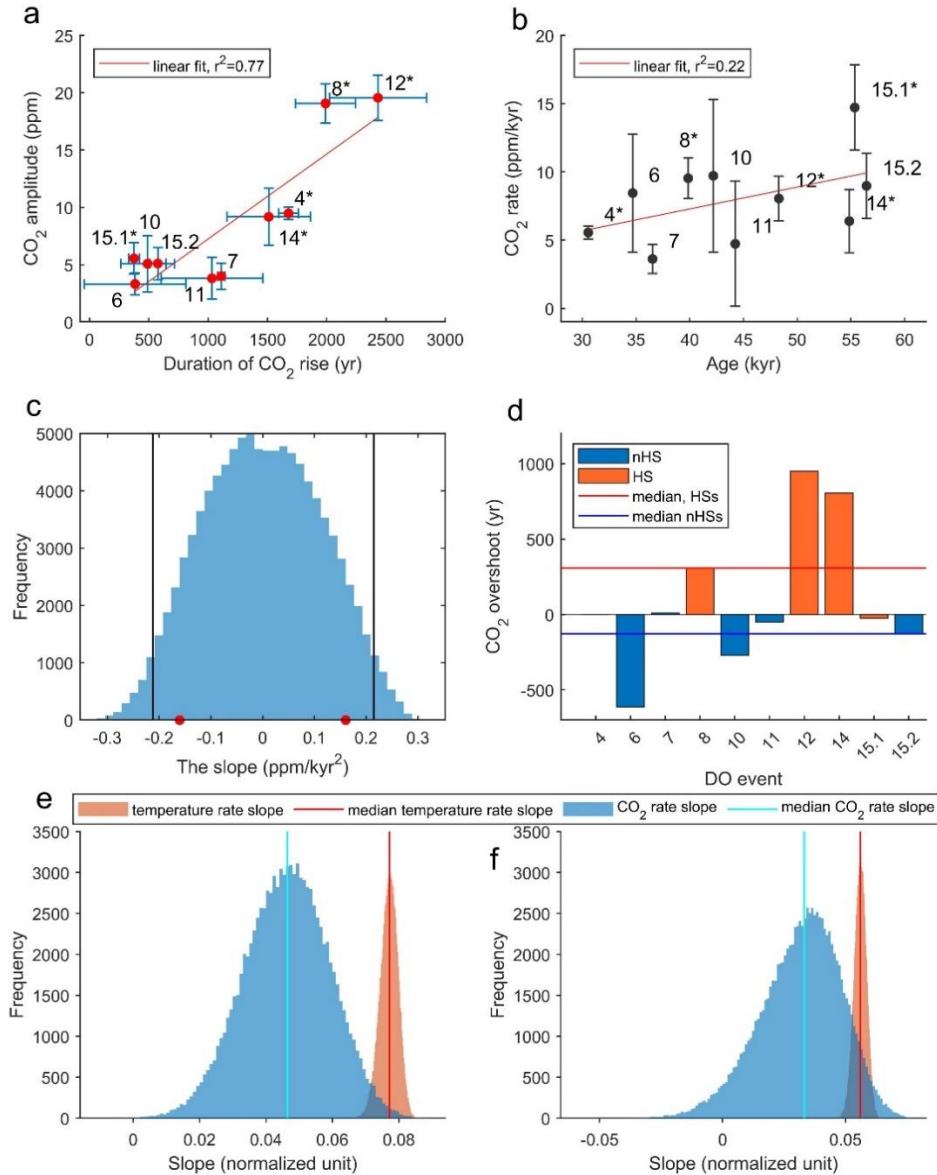
217 In contrast to AIM warming rates, we do not find evidence for a significant decline in the
218 rate of CO₂ rise across the MIS-3 AIM events (with two-side significance 82.7%, Figure 3c).
219 Note that this result is not a statistical artifact due to the low number of CO₂ events resolved by
220 the data, see a one-to-one comparison using only events both analysed in the CO₂ and
221 temperature records in Figure S7. However, the bubble enclosure characteristics of different ice
222 core sites (Bereiter et al., 2012) and the depth/age-dependent ice diffusion (Ahn et al., 2008)
223 could unevenly smooth the composite CO₂ records and bias the CO₂ amplitude. To test the
224 influence of these effects, we perform additional tests and compared the CO₂ and temperature
225 trends for the Talos section of composite CO₂ (Bereiter et al., 2012) vs the Talos $\delta^{18}\text{O}$ data
226 (Landais et al., 2015; Stenni et al., 2011; Supporting Information, Figure S8), and for the newly
227 recovered EDC CO₂ record (Nehrbass-Ahles et al., 2020) spanning 330 to 440 kyr BP vs the
228 EDC δD data (EPICA, 2004), (Supporting Information, Figures S9 and S9). In both cases, the
229 CO₂ trend is less significant than the Antarctic temperature trend (Figure S8, S9). The above
230 experiments are also designed to consider the influence of using different timescales and changes
231 in delta-age (age difference between gas and ice at the same depth, see Supporting Information).
232 The results show that our conclusions are not sensitive to these factors (Supporting Information,
233 Figure S8, S9).

234 Our results are cross-validated by another method that compares the CO₂ and temperature
235 trend: we let the CO₂/temperature rates randomly varying within their uncertainty and repeatedly
236 calculate the slope (without permuting the CO₂/temperature rate data points), after 100,000
237 iterations it turn out the median temperature rate slopes are larger than the CO₂ rate slopes in all

238 CO₂-temperature comparison cases (Five-core $\delta^{18}\text{O}$ vs composite CO₂; Talos CO₂ vs the Talos
239 $\delta^{18}\text{O}$; new EDC CO₂ vs the EDC δD , Supporting Information, Figure 3e, 3f, S11). Overall, these
240 results suggest the rate of CO₂ rise is less sensitive to varying background climate across the
241 MIS-3 than the Antarctic temperature trend.

242 We also do not find a significant difference between the rate of CO₂ rise during HS and
243 nHS (t-test with 95% significance level). However, we do find, consistent with previous work
244 (Bereiter et al., 2012), that CO₂ rise ‘overshoots’ (the excess CO₂ rise time relative to
245 corresponding GS duration) are longer during HS than during nHS (median HS overshoot: 307
246 yr, nHS: -126 yr, Figure 3d). A t-test confirms that the longer overshoots for HS CO₂ rise relative
247 to nHS are significant (at the 95% level). For comparison, we determine the Antarctic warming
248 overshoot in the same way, and no significant difference between HS and nHS is detected (at
249 95% significance level, Figure S1), consistent with a stable north to south lag (Svensson et al.,
250 2020; WAIS, 2015).

251 The CO₂ sensitivity to background climate and H events are similar when detrended CO₂
252 data (removing the long-term signal represented by 20,000 yr smoothing) are used (Supporting
253 Information, Figure S5, S12). To compare with previous research, we also determined the
254 maximums/minimums from a spline fitted CO₂ data with cut off period of 500 yr (Bereiter et al.,
255 2012), again the results hold (Supporting Information, Figure S5, S12).



256

257 **Figure 3. The CO₂ rates and CO₂ overshoot. a.** The CO₂ amplitude vs the duration of CO₂
 258 rises, the error bar marks the 95% CI of the amplitude and duration. **b.** CO₂ rate vs the age of the
 259 CO₂ rise, which is defined by the initiation of the corresponding Greenland stadial. The error bar
 260 marks the 95% CI. **c.** The comparison between the ± 1 time observed CO₂ slope in **b** (red dots)
 261 with the slopes generated by randomly permuting the CO₂ rate. The 2.5% and 97.5% fractile of
 262 the randomly generated slope is marked by vertical black lines. **d.** The CO₂ overshoot. **e.** The

263 distribution of the randomly generated CO₂/temperature rate slopes of five-core averaged $\delta^{18}\text{O}$
264 data (Buizert et al., 2018) and the composite CO₂ data (Bereiter et al., 2015). Note the rates are
265 normalized before fitting the slope. **f.** same as **e** but for the new EDC CO₂ (Nehrbass-Ahles et al.,
266 2020) and EDC δD data (EPICA, 2004).

267

268 **3 Discussion**

269 **3.1. Interpreting the temperature sensitivity**

270 Our statistical analysis suggests the AIM temperature response to the DO cycles is
271 gradually weakened throughout the MIS-3. This result provides a firm quantitative basis for
272 previous suggestions of weakened bipolar connections when climate approaches the glacial
273 maximum (Margari et al., 2010; Mcmanus et al., 1999; Wolff et al., 2009).

274 Recent work indicates that the majority of AIM variability (about 83%) can be explained
275 by a spatially homogeneous oceanic mode (Buizert et al., 2018) that is well captured by the
276 minimum thermodynamic seesaw model (Stocker & Johnsen, 2003). The reduction of the BPS
277 warming rate and $-T_G$ as the climate state cools suggest either a weakening of the mechanisms
278 coupling Antarctic temperature to this oceanic mode and/or a weakening influence of the DO
279 cycles on the Southern Ocean itself. Performing a similar analysis to ours on AIM warming rates
280 observed on surface temperature reconstructions from Southern Ocean marine sediment cores
281 may resolve which is the case.

282 A recent coupled-model investigation of the bipolar seesaw mechanism (Pedro et al.,
283 2018) suggested that during Greenland stadials, the weakened AMOC drives Antarctic warming

284 through the following chain of events: Reduced northward advection of heat in the Atlantic
285 Ocean results in heat accumulation in the South Atlantic. This heat then spreads east around the
286 globe along the northern edge of the Antarctica Circumpolar Current (ACC). As a result, the
287 temperature gradient across the ACC increases, driving an increase in the cross-ACC heat flux
288 carried by ocean eddies. Temperature anomalies south of the ACC are amplified by the retreat of
289 sea ice and the resulting ice-albedo feedback. Finally, heat from the Southern Ocean sea-ice zone
290 is transported to Antarctica by atmospheric eddies, i.e., storms.

291 A cooler background climate state of late MIS-3 (as shown by Antarctic water isotope
292 records (Buizert et al., 2018), or similar trend in ice core noble gas estimates of mean ocean
293 temperature; Bereiter et al., 2018), with thicker Antarctic sea ice, would be expected to reduce
294 the BPS warming rate, because thicker ice would inhibit the ice-albedo feedback (Levermann et
295 al., 2007). Moreover, the concurrent expansion of the sea ice expected in a colder climate would
296 lower the efficiency of atmospheric heat transportation from the warm sea-ice zone to Antarctica,
297 due to the greater distance between Antarctic and the sea-ice-free area. Indeed, marine sediment-
298 core (Collins et al., 2012; Gersonde et al., 2005; Stuut et al., 2004), WDC sea-salt Na record
299 (WAIS, 2015), and climate model (Ferrari et al., 2014), show evidence for Southern Ocean sea-
300 ice expansion at the end of glacial periods.

301

302 **3.2. Interpreting the CO₂ sensitivity**

303 Our results suggest that in contrast to changes in Antarctic temperature the millennial-
304 scale CO₂ rises show little, if any, sensitivity to varying background climate during MIS-3. Our
305 results also show that this less background state-dependent response of CO₂ is also observed in

306 earlier glacial periods (Nehrbass-Ahles et al., 2020; Figure S9), which suggests it is a robust
307 feature of millennial climate variability during glacial periods. Recent studies have suggested
308 that increased Southern Ocean deep convection can jointly explain AIM warming and CO₂
309 trends via the ventilation of heat and CO₂ from ocean depths (Menviel et al., 2018; Skinner et al.,
310 2020). Carbon reservoir age and deep-water temperature reconstructions from the South Atlantic
311 appear to support this ‘Southern Ocean hypothesis’ during HS-4 (Skinner et al., 2020), but do not
312 quantify the scale of its contribution. Furthermore, although strengthened winds are often
313 invoked as the forcing for increased upwelling, Southern Ocean eddies may partially or fully
314 nullify the influence of wind changes on upwelling (Munday et al., 2013). Our results on the
315 different sensitivities of AIM temperature trends and CO₂ to background climate state challenge
316 that a single physical process dominates the millennial signals in both throughout MIS-3.
317 Instead, a dominant influence of Southern Ocean processes on the AIM temperature evolution
318 (Buizert et al., 2018; Pedro et al., 2018) and an important contribution of low- and mid-latitude
319 processes to CO₂, for example by reduction of the biological pump (Nielsen et al., 2019), or CO₂
320 release from terrestrial sources (Bauska et al., 2016; Marcott et al., 2014; Rhodes et al., 2015),
321 would appear consistent with our results.

322 Alternately, the Southern Ocean hypothesis could sidestep our observational constraint if
323 the ventilation of ocean heat is reduced relative to the CO₂ as MIS-3 progresses and the climate
324 cools, or if heat ventilated by deep convection has less influence on Antarctic temperature due,
325 for example, to expanded Antarctic sea ice (Collins et al., 2012; Gersonde et al., 2005; Stuut et
326 al., 2004). In either case, our observations provide a new target for model studies seeking to
327 replicate the millennial-scale variability of temperature and CO₂ and their sensitivities to climate
328 state and H events.

329 The most obvious decoupling of CO₂ and Antarctic temperature occurs during the
330 centennial-scale CO₂ overshoots accompanying H events (Figure 3d). While the CO₂ overshoots
331 are still unexplained, there are a number of candidate mechanisms that would be expected to
332 express a signal in CO₂ and not in Antarctic temperature. Notably, rapid ventilation of
333 accumulated respired carbon from intermediate-depth Atlantic (Chen et al., 2015; Jaccard et al.,
334 2016) and again reduction of the biological pump (Nielsen et al., 2019), or terrestrial CO₂ release
335 (Bauska et al., 2016; Marcott et al., 2014; Rhodes et al., 2015).

337 **Acknowledgments, Samples, and Data**

338 This work was funded by the Natural Science Foundation of China (Grant No. 41290252). JBP
339 and SOR acknowledges support from a Carlsberg Foundation grant to project ChronoClimate.
340 We thank Christo Buizert and Xu Zhang for discussions. ZL and PZ proposed the research. PZ
341 conducted the analyses with support from JBP, MJ and SOR. All authors contributed to the
342 writing of manuscript. The WDC, EDC, EDML, Fuji, Talos $\delta^{18}\text{O}$ in WD2014 timescale, and the
343 five-core averaged $\delta^{18}\text{O}$ data are included in this paper (and its supplementary information files):
344 Buizert, C., Sigl, M., Severi, M., Markle, B. R., Wettstein, J. J., McConnell, J. R., . . .
345 Kawamura, K. (2018). Abrupt ice-age shifts in southern westerly winds and Antarctic climate
346 forced from the north. *Nature*, 563(7733), 681-685. The composite CO₂ data is included in this
347 paper (and its supplementary information files): Bereiter, B., Eggleston, S., Schmitt, J., Nehrbass
348 Ahles, C., Stocker, T. F., Fischer, H., . . . Chappellaz, J. (2015). Revision of the EPICA Dome C
349 CO₂ record from 800 to 600 kyr before present. *Geophysical Research Letters*, 42(2), 542-549.
350 The new EDC CO₂ data is included in this paper (and its supplementary information files):

351 Nehrbaas-Ahles, C., Shin, J., Schmitt, J., Bereiter, B., Joos, F., Schilt, A., . . . Grilli, R. (2020).
352 Abrupt CO₂ release to the atmosphere under glacial and early interglacial climate conditions.
353 *Science*, 369(6506), 1000-1005. The EDC δ D data is included in this paper (and its
354 supplementary information files): EPICA. (2004). Eight glacial cycles from an Antarctic ice
355 core. *Nature*, 429(6992), 623-628.

356

357 **References**

- 358 1. Ahn, J., & Brook, E. J. (2014). Siple Dome ice reveals two modes of millennial CO₂ change during the last ice
359 age. *Nature Communications*, 5(4), 4723.
- 360 2. Ahn, J., Headly, M., Wahlen, M., Brook, E. J., Mayewski, P. A., & Taylor, K. C. (2008). CO₂ diffusion in
361 polar ice: observations from naturally formed CO₂ spikes in the Siple Dome (Antarctica) ice core. *Journal of*
362 *Glaciology*, 54(187), 685-695.
- 363 3. Anderson, R. F., Ali, S., Bradtmiller, L. I., Nielsen, S. H., Fleisher, M. Q., Anderson, B. E., & Burckle, L. H.
364 (2009). Wind-driven upwelling in the Southern Ocean and the deglacial rise in atmospheric CO₂. *Science*,
365 323(5920), 1443-1448.
- 366 4. Anderson, R. F., & Carr, M.-E. (2010). Paleoclimate. Uncorking the Southern Ocean's vintage CO₂. *Science*,
367 328(5982), 1117-1118.
- 368 5. Bauska, T. K., Baggenstos, D., Brook, E. J., Mix, A. C., & Lee, J. E. (2016). Carbon isotopes characterize
369 rapid changes in atmospheric carbon dioxide during the last deglaciation. *Proc Natl Acad U S A*, 113(13),
370 3465-3470.
- 371 6. Bauska, T. K., Brook, E. J., Marcott, S. A., Baggenstos, D., Shackleton, S., Severinghaus, J. P., & Petrenko, V.
372 V. (2018). Controls on Millennial-Scale Atmospheric CO₂ Variability During the Last Glacial Period.
373 *Geophysical Research Letters*, 45(15), 7731-7740. doi:10.1029/2018GL077881

- 374 7. Bereiter, B., Eggleston, S., Schmitt, J., Nehrbass Ahles, C., Stocker, T. F., Fischer, H., . . . Chappellaz, J.
375 (2015). Revision of the EPICA Dome C CO₂ record from 800 to 600 kyr before present. *Geophysical Research*
376 *Letters*, *42*(2), 542-549.
- 377 8. Bereiter, B., Lüthi, D., Siegrist, M., Schüpbach, S., Thomas F, S., & Fischer, H. (2012). Mode change of
378 millennial CO₂ variability during the last glacial cycle associated with a bipolar marine carbon seesaw.
379 *Proceedings of the National Academy of Sciences of the United States of America*, *109*(25), 9755-9760.
- 380 9. Bereiter, B., Shackleton, S., Baggenstos, D., Kawamura, K., & Severinghaus, J. (2018). Mean global ocean
381 temperatures during the last glacial transition. *Nature*, *553*(7686), 39-44.
- 382 10. Buizert, C., Cuffey, K. M., Severinghaus, J. P., Baggenstos, D., Fudge, T. J., Steig, E. J., . . . Brook, E. J.
383 (2015). The WAIS Divide deep ice core WD2014 chronology – Part 1: Methane synchronization (68–31 ka
384 BP) and the gas age–ice age difference. *Climate of the Past*, *11*(4), 153-173.
- 385 11. Buizert, C., Sigl, M., Severi, M., Markle, B. R., Wettstein, J. J., McConnell, J. R., . . . Kawamura, K. (2018).
386 Abrupt ice-age shifts in southern westerly winds and Antarctic climate forced from the north. *Nature*,
387 *563*(7733), 681-685.
- 388 12. Capron, E., Landais, A., Chappellaz, J., Schilt, A., & Stenni, B. (2010). Millennial and sub-millennial scale
389 climatic variations recorded in polar ice cores over the last glacial period. *Climate of the Past Discussions*,
390 *6*(1), 345-365.
- 391 13. Chen, T., Robinson, L. F., Burke, A., Southon, J., Spooner, P., Morris, P. J., & Ng, H. C. (2015). Synchronous
392 centennial abrupt events in the ocean and atmosphere during the last deglaciation. *Science*, *349*, 1537-1541.
- 393 14. Collins, L. G., Pike, J., Allen, C. S., & Hodgson, D. A. (2012). High - resolution reconstruction of southwest
394 Atlantic sea - ice and its role in the carbon cycle during marine isotope stages 3 and 2. *Paleoceanography*,
395 *27*(3), PA3217.
- 396 15. EPICA. (2004). Eight glacial cycles from an Antarctic ice core. *Nature*, *429*(6992), 623-628.
- 397 16. EPICA. (2006). One-to-one coupling of glacial climate variability in Greenland and Antarctica. *Nature*,
398 *444*(7116), 195-198.
- 399 17. Ferrari, R., Jansen, M. F., Adkins, J. F., Burke, A., Stewart, A. L., & Thompson, A. F. (2014). Antarctic sea ice
400 control on ocean circulation in present and glacial climates. *Proceedings of the National Academy of Sciences*,
401 *111*(24), 8753-8758.

- 402 18. Gersonde, R., Crosta, X., Abelmann, A., & Armand, L. (2005). Sea-surface temperature and sea ice
403 distribution of the Southern Ocean at the EPILOG Last Glacial Maximum—a circum-Antarctic view based on
404 siliceous microfossil records. *Quaternary Science Reviews*, *24*(7), 869-896.
- 405 19. Gottschalk, J., Battaglia, G., Fischer, H., Frölicher, T. L., Jaccard, S. L., Jeltsch-Thömmes, A., . . . Stocker, T.
406 F. (2019). Mechanisms of millennial-scale atmospheric CO₂ change in numerical model simulations.
407 *Quaternary Science Reviews*, *220*, 30-74. doi:<https://doi.org/10.1016/j.quascirev.2019.05.013>
- 408 20. Jaccard, S. L., Galbraith, E. D., Martínez-García, A., & Anderson, R. F. (2016). Covariation of deep Southern
409 Ocean oxygenation and atmospheric CO₂ through the last ice age. *Nature*, *530*(7589), 207–210.
- 410 21. Jouzel, J., Delaygue, G., Amaelle, L., Valerie, M.-D., Risi, C., & Vimeux, F. (2013). Water isotopes as tools
411 to document oceanic sources of precipitation. *Water Resources Research*, *49*(11), 7469-7486.
- 412 22. Kawamura, K., Parrenin, F., Lisiecki, L., Uemura, R., Vimeux, F., Severinghaus, J. P., . . . Jouzel, J. (2007).
413 Northern Hemisphere forcing of climatic cycles in Antarctica over the past 360,000 years. *Nature*, *448*(7156),
414 912-916.
- 415 23. Kindler, P., Guillevic, M., Baumgartner, M. F., Schwander, J., Landais, A., & Leuenberger, M. (2014).
416 Temperature reconstruction from 10 to 120 kyr b2k from the NGRIP ice core. *Climate of the Past*, *10*(2), 887-
417 902.
- 418 24. Landais, A., Masson-Delmotte, V., Stenni, B., Selmo, E., Roche, D. M., Jouzel, J., . . . Arzel, O. (2015). A
419 review of the bipolar see-saw from synchronized and high resolution ice core water stable isotope records from
420 Greenland and East Antarctica. *Quaternary Science Reviews*, *114*, 18-32.
- 421 25. Levermann, A., Schewe, J., & Montoya, M. (2007). Lack of bipolar see-saw in response to Southern Ocean
422 wind reduction. *Geophysical Research Letters*, *34*(34), 195-225.
- 423 26. Marcott, S. A., Bauska, T. K., Buizert, C., Steig, E. J., Rosen, J. L., Cuffey, K. M., . . . Kalk, M. L. (2014).
424 Centennial-scale changes in the global carbon cycle during the last deglaciation. *Nature*, *514*(7524), 616–619.
- 425 27. Margari, V., Skinner, L. C., Tzedakis, P. C., Ganopolski, A., Vautravers, M., & Shackleton, N. J. (2010). The
426 nature of millennial-scale climate variability during the past two glacial periods. *Nature Geoscience*, *3*(2), 127-
427 131.
- 428 28. Mcmanus, J. F., Oppo, D. W., & Cullen, J. L. (1999). A 0.5-Million-Year Record of Millennial-Scale Climate
429 Variability in the North Atlantic. *Science*, *283*(5404), 971-975.

- 430 29. Menviel, L., Spence, P., & England, M. H. (2015). Contribution of enhanced Antarctic Bottom Water
431 formation to Antarctic warm events and millennial-scale atmospheric CO₂ increase. *Earth and Planetary*
432 *Science Letters*, 413, 37-50.
- 433 30. Menviel, L., Spence, P., Yu, J., Chamberlain, M. A., Matear, R. J., Meissner, K. J., & England, M. H. (2018).
434 Southern Hemisphere westerlies as a driver of the early deglacial atmospheric CO₂ rise. *Nature*
435 *communications*, 9(1), 2503.
- 436 31. Munday, D. R., Johnson, H. L., & Marshall, D. P. (2013). Eddy saturation of equilibrated circumpolar currents.
437 *Journal of Physical Oceanography*, 43(3), 507-532.
- 438 32. Nehrbass-Ahles, C., Shin, J., Schmitt, J., Bereiter, B., Joos, F., Schilt, A., . . . Grilli, R. (2020). Abrupt CO₂
439 release to the atmosphere under glacial and early interglacial climate conditions. *Science*, 369(6506), 1000-
440 1005.
- 441 33. NGRIP. (2004). High-resolution record of Northern Hemisphere climate extending into the last interglacial
442 period. *Nature*, 431(7005), 147–151.
- 443 34. Nielsen, S. B., Jochum, M., Pedro, J. B., Eden, C., & Nuterman, R. (2019). Two - Timescale Carbon Cycle
444 Response to an AMOC Collapse. *Paleoceanography and Paleoclimatology*, 34(4), 511-523.
- 445 35. Pedro, J. B., Jochum, M., Buizert, C., He, F., Barker, S., & Rasmussen, S. O. (2018). Beyond the bipolar
446 seesaw: Toward a process understanding of interhemispheric coupling. *Quaternary Science Reviews*, 192, 27-
447 46.
- 448 36. Rasmussen, S. O., Bigler, M., Blockley, S. P., Blunier, T., Buchardt, S. L., Clausen, H. B., . . . Fischer, H.
449 (2014). A stratigraphic framework for abrupt climatic changes during the Last Glacial period based on three
450 synchronized Greenland ice-core records: refining and extending the INTIMATE event stratigraphy.
451 *Quaternary Science Reviews*, 106, 14-28.
- 452 37. Rhodes, R. H., Brook, E. J., Chiang, J. C., Blunier, T., Maselli, O. J., McConnell, J. R., . . . Severinghaus, J. P.
453 (2015). Paleoclimate. Enhanced tropical methane production in response to iceberg discharge in the North
454 Atlantic. *Science*, 348(6238), 1016-1019.
- 455 38. Skinner, L., Menviel, L., Broadfield, L., Gottschalk, J., & Greaves, M. (2020). Southern Ocean convection
456 amplified past Antarctic warming and atmospheric CO₂ rise during Heinrich Stadial 4. *Communications Earth*
457 *& Environment*, 1(1), 1-8.

- 458 39. Stenni, B., Buiron, D., Frezzotti, M., Albani, S., Barbante, C., Bard, E., . . . Bonazza, M. (2011). Expression of
 459 the bipolar see-saw in Antarctic climate records during the last deglaciation. *Nature Geoscience*, 4(1), 46-49.
- 460 40. Stocker, T. F., & Johnsen, S. J. (2003). A minimum thermodynamic model for the bipolar seesaw.
 461 *Paleoceanography*, 18(4), 1087.
- 462 41. Stuut, J. B. W., Crosta, X., Borg, K. V. D., & Schneider, R. (2004). Relationship between Antarctic sea ice and
 463 southwest African climate during the late Quaternary. *Geology*, 32(10), 909-912.
- 464 42. Svensson, A., Andersen, K. K., Bigler, M., Clausen, H. B., Dahljensen, D., Davies, S. M., . . . Rasmussen, S.
 465 O. (2008). A 60 000 year Greenland stratigraphic ice core chronology. *Climate of the Past Discussions*, 3(6),
 466 47-57.
- 467 43. Svensson, A., Dahl-Jensen, D., Steffensen, J. P., Blunier, T., Rasmussen, S. O., Vinther, B. M., . . . Bigler, M.
 468 (2020). Bipolar volcanic synchronization of abrupt climate change in Greenland and Antarctic ice cores during
 469 the last glacial period. *Clim. Past*, 16(4), 1565-1580. doi:10.5194/cp-16-1565-2020
- 470 44. Thompson, A. F., Hines, S. K., & Adkins, J. F. (2019). A Southern Ocean Mechanism for the Interhemispheric
 471 Coupling and Phasing of the Bipolar Seesaw. *Journal of Climate*, 32(14), 4347-4365.
- 472 45. Toggweiler, J. R., Russell, J. L., & Carson, S. R. (2006). Midlatitude westerlies, atmospheric CO₂, and climate
 473 change during the ice ages. *Paleoceanography*, 21(2), PA2005.
- 474 46. Veres, D., Bazin, L., Landais, A., Toyé Mahamadou Kele, H., Lemieux-Dudon, B., Parrenin, F., . . . Capron, E.
 475 (2013). The Antarctic ice core chronology (AICC2012): an optimized multi-parameter and multi-site dating
 476 approach for the last 120 thousand years. *Climate of the Past*, 9(4), 1733-1748.
- 477 47. WAIS, D. P. M. (2013). Onset of deglacial warming in West Antarctica driven by local orbital forcing. *Nature*,
 478 500(7463), 440-444.
- 479 48. WAIS, D. P. M. (2015). Precise inter-polar phasing of abrupt climate change during the last ice age. *Nature*,
 480 520(7549), 661-665.
- 481 49. Watanabe, O., Jouzel, J., Johnsen, S., Parrenin, F., Shoji, H., & Yoshida, N. (2003). Homogeneous climate
 482 variability across East Antarctica over the past three glacial cycles. *Nature*, 422(6931), p. 509-512.
- 483 50. Wolff, E. W., Fischer, H., & Röthlisberger, R. (2009). Glacial terminations as southern warmings without
 484 northern control. *Nature Geoscience*, 2(3), 206-209.

485 **References From the Supporting Information**

- 486 51. Ahn, J., Headly, M., Wahlen, M., Brook, E. J., Mayewski, P. A., & Taylor, K. C. (2008). CO₂ diffusion in
 487 polar ice: observations from naturally formed CO₂ spikes in the Siple Dome (Antarctica) ice core. *Journal of*
 488 *Glaciology*, *54*(187), 685-695.
- 489 52. Bereiter, B., Eggleston, S., Schmitt, J., Nehrbass Ahles, C., Stocker, T. F., Fischer, H., . . . Chappellaz, J.
 490 (2015). Revision of the EPICA Dome C CO₂ record from 800 to 600 kyr before present. *Geophysical Research*
 491 *Letters*, *42*(2), 542-549.
- 492 53. Bereiter, B., Lüthi, D., Siegrist, M., Schüpbach, S., Thomas F, S., & Fischer, H. (2012). Mode change of
 493 millennial CO₂ variability during the last glacial cycle associated with a bipolar marine carbon seesaw.
 494 *Proceedings of the National Academy of Sciences of the United States of America*, *109*(25), 9755-9760.
- 495 54. Buizert, C., Sigl, M., Severi, M., Markle, B. R., Wettstein, J. J., McConnell, J. R., . . . Kawamura, K. (2018).
 496 Abrupt ice-age shifts in southern westerly winds and Antarctic climate forced from the north. *Nature*,
 497 *563*(7733), 681-685.
- 498 55. EPICA. (2004). Eight glacial cycles from an Antarctic ice core. *Nature*, *429*(6992), 623-628.
- 499 56. Landais, A., Masson-Delmotte, V., Stenni, B., Selmo, E., Roche, D. M., Jouzel, J., . . . Arzel, O. (2015). A
 500 review of the bipolar see-saw from synchronized and high resolution ice core water stable isotope records from
 501 Greenland and East Antarctica. *Quaternary Science Reviews*, *114*, 18-32.
- 502 57. Nehrbass-Ahles, C., Shin, J., Schmitt, J., Bereiter, B., Joos, F., Schilt, A., . . . Grilli, R. (2020). Abrupt CO₂
 503 release to the atmosphere under glacial and early interglacial climate conditions. *Science*, *369*(6506), 1000-
 504 1005.
- 505 58. Stenni, B., Buiron, D., Frezzotti, M., Albani, S., Barbante, C., Bard, E., . . . Bonazza, M. (2011). Expression of
 506 the bipolar see-saw in Antarctic climate records during the last deglaciation. *Nature Geoscience*, *4*(1), 46-49.
- 507 59. Svensson, A., Andersen, K. K., Bigler, M., Clausen, H. B., Dahljensen, D., Davies, S. M., . . . Rasmussen, S.
 508 O. (2008). A 60 000 year Greenland stratigraphic ice core chronology. *Climate of the Past Discussions*, *3*(6),
 509 47-57.
- 510 60. Veres, D., Bazin, L., Landais, A., Toyé Mahamadou Kele, H., Lemieux-Dudon, B., Parrenin, F., . . . Capron, E.
 511 (2013). The Antarctic ice core chronology (AICC2012): an optimized multi-parameter and multi-site dating
 512 approach for the last 120 thousand years. *Climate of the Past*, *9*(4), 1733-1748.